

Evaluation of RSM-Simulated Precipitation During CEOP

I. MEINKE, J. ROADS, and M. KANAMITSU

*Experimental Climate Prediction Center, Scripps Institution of Oceanography, University of California,
San Diego, La Jolla, CA 92093-0224, USA*

(Manuscript received 1 February 2006, in final form 1 November 2006)

Abstract

Precipitation simulated using the Regional Spectral Model (RSM) during the Coordinated Enhanced Observing Period (CEOP; July 1, 2001 to December 31, 2004) is evaluated by transferring the RSM to seven different regions of the globe and comparing the simulations with observations. These regions cover the eight Continental-Scale Experiments (CSEs) of the Global Energy and Water-cycle EXperiment (GEWEX) and encompass a broad variety of physical and dynamical meteorological processes. Gridded observations of the Global Precipitation Climatology Project (GPCP) and the Global Precipitation Climatology Center (GPCC), as well as CEOP reference site precipitation observations are compared with the RSM simulated precipitation for the first half of the CEOP Enhanced Observation Period (EOP) III (October 2002 to March 2003). After estimating the uncertainty ranges of both the model and the observations, model deficiencies were obtained for almost all model domains in terms of the amount of simulated precipitation. Although the RSM is able to accurately simulate the seasonal evolution and spatial distribution of precipitation, the RSM has an almost uniform positive bias (i.e., RSM values are greater than observed values) over almost all the domains. Most of the positive bias is associated with convection in the Intertropical Convergence Zone (ITCZ) or monsoonal convection in Southeast Asia. Predicted stratiform precipitation is also excessive over areas of elevated topography. As the control simulations used a Relaxed Arakawa–Schubert scheme (RAS), sensitivity tests with three additional convection schemes were then carried out to assess whether the simulations could be improved. The additional convection schemes were: 1) the Simplified Arakawa–Schubert scheme (SAS); 2) the Kain–Fritsch scheme (KF); and 3) the National Centers for Atmospheric Research (NCAR) Community Climate Model (CCM) scheme. The precipitation simulation was significantly improved for almost all domains when using either the KF scheme or the SAS scheme. The best simulations of ITCZ convective precipitation and Southeast Asian monsoon convective precipitation were achieved using the SAS convection scheme.

1. Introduction

Regional simulations of the water and energy cycles are sensitive to the way in which physical and dynamical processes are represented in the chosen model. As the dominance of dynamical and physical processes vary in different regions of the globe, parameterization assump-

tions used for a particular regional model may provide good results for one region but poor results for other regions with contrasting climatic regimes. This sensitivity may become especially important for regional climate-change scenarios. To ensure that regional models are capable of assessing the regional consequences of global climate change, extensive evaluations are needed for many different climatological conditions. Accordingly, transferability studies such as the Inter-Continental Scale Experiment Transferability Study (ICTS; Rockel et al. 2005), whereby a regional model is transferred

Corresponding author: Dr. Insa Meinke, GKSS,
Max-Planck Str. 1, 21502 Geesthacht, Germany.
Email: imeinke@ucsd.edu
© 2007, Meteorological Society of Japan

to several unique regional domains with unique climates, may eventually become an increasingly important evaluation methodology.

The aim of this particular transferability study is to evaluate the ability of the Regional Spectral Model (RSM) of the Experimental Climate Prediction Center (ECPC) to simulate precipitation over a large number of different regional domains. In particular, numerical simulations are conducted for regional climates in tropical, subtropical, mid-latitude, and polar regions, which all include small-scale convective systems and various large-scale circulation regimes such as monsoons, the ITCZ, and mid-latitude storms. These simulations are then systematically compared with GPCP and GPCC gridded observations as well as measurements undertaken at CEOP reference sites.

It should be noted that many international model comparisons (e.g., Takle et al. 2006) and precipitation evaluation experiments have been carried out previously; some have included older versions of the RSM. Briefly, Hong and Letma (1999) found a tendency for the RSM to simulate excessive precipitation, and Roads et al. (2003a) found that the RSM seasonal systematic precipitation error over South America was similar to the systematic error in the driving NCEP/NCAR reanalysis. Chen et al. (1999) demonstrated that the RSM is especially advantageous for intense precipitation events at regional spatial scales over California.

Differences between simulated and observed precipitation result from a number of factors, including uncertainties in the observations and simulation uncertainties that are not necessarily part of the model. To ensure that the differences between the model predictions and observations represent the true model deficiency, the magnitude of these uncertainties must be considered (e.g., Vidale et al. 2003; Meinke et al. 2004, and Meinke 2006). In the present study, we found that the RSM has a positive precipitation bias over most regional domains. This positive bias is associated with both convective and stratiform precipitation. Sensitivity tests were then carried out using four different convection schemes for the months with the largest differences. As is discussed below, different parameterizations work best for different domains and their characteristic meteorological conditions. This suggests that until a more universal con-

vective parameterization can be developed, it may still be best for regional simulations to use particular parameterizations; however, there does appear to be at least two parameterizations (SAS and KF) that provide reasonable results for most domains for the particular horizontal resolution used in this version of the RSM (approximately 50 km and 28 vertical levels).

2. Regional Spectral Model (RSM)

2.1 Model features

The Regional Spectral Model (RSM) was initially developed by Juang and Kanamitsu (1994) (see also Juang et al. 1997) to provide a regional scale extension to the parent Global Spectral Model (GSM; Kalnay et al. 1996). In principle, the RSM provides an almost seamless transition to the GSM or associated NCEP reanalyses (Kalnay et al. 1996; Kanamitsu et al. 2002) and the high resolution region of interest.

An intrinsic advantage of the RSM, according to Hong and Leetma (1999), is that compared with other regional climate models it places few restrictions on nesting size. Smaller nests are easily embedded within the large-scale reanalysis or GSM forecasts without noticeable boundary errors or influence. Both the GSM and RSM use the same primitive equation system of prognostic equations for virtual temperature, humidity, surface pressure, and mass continuity in terrain-following sigma coordinates (sigma is defined as the ratio of the ambient pressure to surface pressure). Therefore, in the absence of any regional forcing, intrinsic internal dynamics, significant differences in physical parameterization, or differences in spatial resolution, the RSM solution should be identical to the GSM solution. A minor structural difference between the two models is that the GSM utilizes vorticity and divergence equations, whereas the RSM utilizes momentum equations to ensure simple lateral boundary conditions. The horizontal basis functions of the GSM and RSM are also different. The GSM uses spherical harmonics with a triangular truncation of T62, whereas the RSM uses cosine or sine waves to represent regional perturbations about the imposed global scale base fields on the regional grids. The sine and cosine spectral representations are carefully chosen to ensure that the normal wind perturbations

are anti-symmetric about the lateral boundary. Other model scalar variables (i.e., virtual temperature, specific humidity, and surface log pressure) use symmetric perturbations. A number of papers have described the capability of RSM regional simulations (Chen et al. 1999; Anderson et al. 2000a,b; Anderson et al. 2001; Anderson and Roads 2002; Han and Roads 2004; Roads and Chen 2000; Roads et al. 2003a,b,c; Roads 2004a,b; Takle et al. 1999). The results of these studies demonstrate that the RSM is useful for simulating and understanding regional climates. The RSM, like other regional models, provides an increased focus for specific regions, can be constrained by realistic large scale conditions, and is able to make use of higher resolution regional data sets in carrying out evaluations.

2.2 Experiment setup

The RSM runs were carried out on a $0.5^\circ \times 0.5^\circ$ latitude–longitude grid upon a Mercator projection. Initial and boundary conditions derived from NCEP Reanalyses II (Kanamitsu et al. 2002) were used to force the RSM.

The initial simulation period was from July 1999 to December 2004. Although the period of interest in this study covers the period from October 2002 to March 2003, the simulations were initiated 3.25 years earlier than this date because the land surface model is required to be equilibrated. The global average surface water of the NCEP Global Spectral Model (GSM) was equilibrated after approximately 3 years (see Roads et al. 1999). Similarly long damping time-scales were used for the surface water in these runs.

The RSM was run over seven different computational domains located over the eight different CSEs.

The rectangles in Fig. 1 indicate the model domains, including the boundary zones. One domain covers the Mackenzie GEWEX Study (MAGS) region; a second covers the GEWEX Americas Prediction Project (GAPP) and was defined by the Project for Intercomparison of Regional Climate Simulations (PIRCS; Takle et al. 1999). A third domain covers both, the Large-Scale Biosphere–Atmosphere Experiment in Amazonia (LBA) and the La Plata Ba-

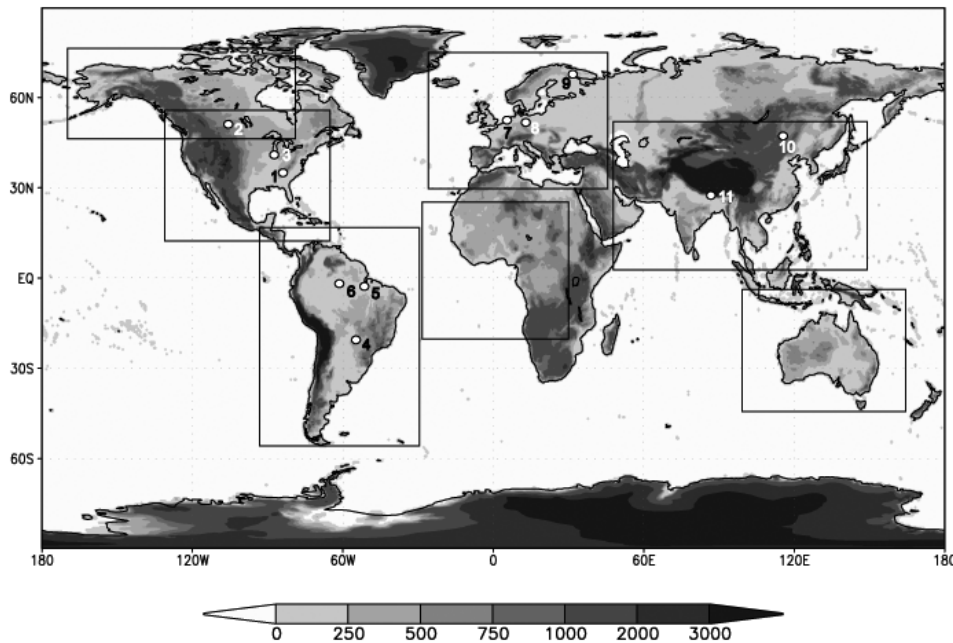


Fig. 1. Model domains (rectangles) and CEOP reference sites used in this study: 1, Oak Ridge; 2, Ft. Peck; 3, Bondville; 4, Pantnanal; 5, Manaus; 6, Santarem; 7, Cabauw; 8, Lindenberg; 9, Sodankylä; 10, Mongolia; 11, Himalayas. The reference sites that are not numbered are not taken into account.

sin (LPB) region, which was used for a previous South America intercomparison (e.g., Roads et al. 2003a). A fourth domain over Europe includes the BALTEX catchment area, taken from the definition of the Climate version of the Lokal Model (CLM) area used for the European Union (EU) project “Prediction of Regional scenarios and Uncertainties for Defining European Climate change risks and Effects” (PRUDENCE; Christensen et al. 2005; Christensen et al. 2006). The fifth domain, over Africa, covers the African Monsoon Multidisciplinary Analysis (AMMA) region, and the sixth domain, over Asia, covers the GEWEX Asian Monsoon Experiment (GAME) region, expanded to cover the Himalayan CEOP reference site. The selection of the seventh domain, the MDB (Murray-Darling-Basin Water Budget Project) area, was based on a previous case study that was part of the GEWEX Cloud System Study (GCSS; Ryan et al. 2000). In the following text, the seven model domains are named after their corresponding CSE, as described above: AMMA, BALTEX, GAME, GAPP, LBA, MAGS, and MDB.

2.3 Uncertainties related to the initial and boundary conditions

As discussed in previous studies (e.g., Meinke et al. 2004; Meinke 2006) there are two major factors that lead to uncertainties in the evaluation of regional simulations. The first is uncertainties in the observation data used to evaluate the simulation results. The second is uncertainties in the initial state and boundary conditions used for the regional model runs (Vidale et al. 2003; Palmer 2000).

To crudely assess uncertainties in the initial and boundary conditions used as forcing, we carried out two short-term realizations by initializing the second set of model runs (for all seven domains) 1 day later than the first set. Monthly means for each model run were then calculated to assess the uncertainty ranges for each domain (see Appendix I). To avoid inconsistencies related to the model boundaries, the values of the eight outer grid boxes (sponge zone) in the model are not taken into account.

Figure 2 shows the root mean square (*RMS*) differences of simulated monthly mean precipitation for each domain. The largest differences

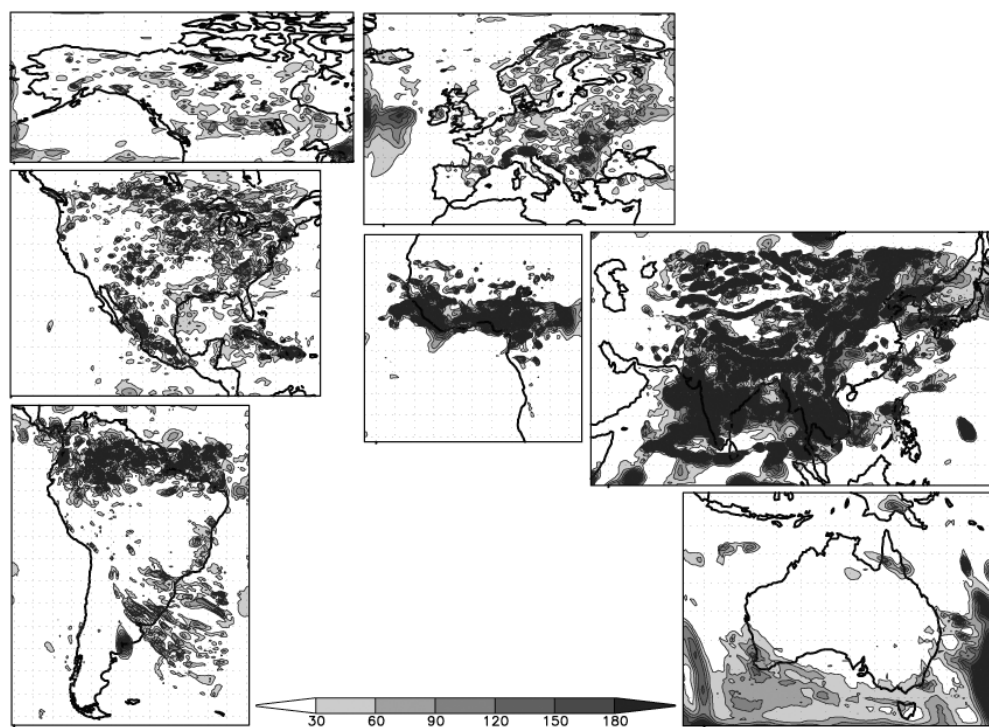


Fig. 2. Root mean square differences between two RSM runs [mm month^{-1}] (precipitation sum) with slightly different initial conditions.

Table 1. Uncertainty ranges of monthly mean precipitation [mm], area means, October 2002 to March 2003.

	Initial Condition	Observation (GPCP)	Combined uncertainty ranges
MAGS	2.8	10.7	11.1
GAPP	4.1	1.8	4.5
LBA	3.9	24.1	24.4
BALTEX	0.5	17.6	17.6
GAME	5.6	6.5	8.6
AMMA	2	11.4	11.5
MDB	1.2	6.0	6.2

occur over the GAME region, which is the largest domain. In other regions, the *RMS* differences are large over the ITCZ (see the simulations over the AMMA and LBA domains). In domains where the ITCZ has no direct impact, the rms differences are smaller. The mean uncertainty ranges for each domain are calculated in the manner described in Appendix I and are shown in Table 1. As expected from the rms differences, the GAME domain has the largest uncertainty range (5.6 mm month⁻¹). The smallest uncertainty range was recorded for the BALTEX domain.

3. Observational data used in the evaluation

3.1 GPCP data

The Global Precipitation Climatology Project (GPCP) was initially established to provide monthly mean precipitation data on a global 2.5° × 2.5° latitude–longitude grid. Monthly mean precipitation estimates have been produced since 1979 and were planned to continue until 2005. In addition to the monthly mean data, a 2.5° × 2.5° pentad data set (from 1979) and a 1° × 1° daily data set (from 1997) are also available. To enable a comparison of the two data sets, the 1° × 1° daily data set was interpolated to a 0.5° × 0.5° latitude–longitude grid on a Mercator projection.

The GPCP data set merges infrared and microwave satellite estimates of precipitation with rain gauge data from more than 6,000

stations. Infrared precipitation estimates are obtained from GOES (United States), GMS (Japan), and Meteosat (European Community) geostationary satellites and National Oceanic and Atmospheric Administration (NOAA) operational polar-orbiting satellites. Microwave estimates are obtained from the U.S. Defense Meteorological Satellite Program (DMSP) satellites using the Special Sensor Microwave Imager (SSM/I). Details of the component data sets and the method used to merge these data are provided by Huffman et al. (1997) and Adler et al. (2003).

3.2 HOAPS/GPCC

Data from the Hamburg Ocean Atmosphere Parameter Set (HOAPS; Grassl et al. 2000) are a multi-satellite product consisting of all available Single Scattering Microwave Interferometer (SSM/I) instruments providing utilizable data. In addition to global precipitation, the HOAPS data set contains global fields of turbulent heat fluxes, evaporation minus precipitation, and all of the basic state variables required for the derivation of these fluxes. The variables are derived from SSM/I and AVHRR (Advanced Very High Resolution Radiometer) satellite data over the ice-free ocean obtained between July 1987 and December 2002. The default spatial resolution of HOAPS-G is 0.5°, including pentad, monthly, and climatologically monthly means.

As the HOAPS data set does not contain data over land, it has traditionally included gridded rain-gauge data from the Global Precipitation Climatology Centre (GPCC) (Rudolf et al. 2003). The GPCC interpolation method is based on an inverse distance-weighting scheme, taking the directional distribution (clustering) of stations into account. The construction of gridded fields of area-averaged precipitation consists of two major steps: 1) interpolation of the irregularly distributed rain-gauge observations to the points of a regular grid, and 2) conversion of the grid point values to area averages for each grid box. The area-averaged precipitation for a 0.5° grid can then be calculated (Schneider and Rudolph 2003).

3.3 CEOP in situ measurements

The CEOP in situ data include reference sites from all of the CSE regions, which cover most of the global land regions. These reference

sites are well-instrumented locations of small- to intermediate-scale areas (10^4 km² or less). There are currently four different enhanced observation periods (EOP). The period of interest in this study was selected on the basis of two criteria: 1) The EOP that contains data from the greatest number of reference sites, and 2) the EOP that covers the longest time-span. At the time of the beginning of this study, these criteria were best fulfilled by the first half of EOP III, for which the data sets from 11 CEOP reference sites were available for the period from October 2002 to March 2003.

3.4 Observational uncertainties

a GPCP precipitation observations

To assess the uncertainty range of the observations, at least one other data set is required. In this study, the uncertainty ranges of the GPCP data were calculated according to the method described in Appendix I, by comparing GPCP data with HOAPS/GPCC data. To ensure that these uncertainty ranges are comparable with the simulations, the area of the eight outer model grid boxes is not taken into account. The uncertainty ranges of the GPCP data for each domain are shown in Table 1. The largest uncertainty range is estimated for LBA (24.1 mm month⁻¹), followed by BALTEX (17.6 mm month⁻¹). Small uncertainty ranges are assessed for GAPP, MDB, and GAME.

The combined uncertainty ranges of both the observations and the initial and boundary conditions (see Section 2.3) are largest for LBA and BALTEX, whereas small combined uncertainty ranges are indicated for MDB and GAPP. All of the uncertainty ranges shown in Table 1 are area averages. In this regard, the CEOP station measurements are very useful in obtaining an insight into the meteorological conditions at a particular model grid point within each domain.

b CEOP station observations

There has been a large amount of discussion on the merits of comparing point values with gridded data sets (e.g., Mearns et al. 1995; Osborn and Hulme 1998; Skelley and Henderson-Sellers 1996). In particular, Osborn and Hulme (1998) demonstrated that simulated precipitation events should be viewed as area averages for each grid box, as parameterizations of surface fluxes and precipitation processes are typi-

cally developed to represent the statistics of an area rather than a point. Thus, the comparison of simulated precipitation with point measurements involves uncertainties related to the different degrees of representativeness of the various spatial scales. In this study, we estimate this uncertainty by comparing CEOP precipitation measurements with GPCC data taken from the HOAPS/GPCC data set. Both data sets consist of gauge measurements of precipitation. GPCC data, however, is a gridded data set (see Schneider and Rudolph 2003). For each grid box that contains a CEOP reference site, the uncertainty is calculated according to the method described in Appendix I.

As shown in Fig. 2, the uncertainty of the initial and boundary conditions is spatially inhomogeneous. Thus, we also estimate the uncertainty ranges of the initial condition for each grid box that contains a CEOP reference site; the results are shown in Table 2. As shown in Table 1, the combined uncertainty range for the LBA area mean shows the largest value of all the domains. The estimates of uncertainty ranges for single CEOP stations reflect the spatial inhomogeneity. For example, the combined range of uncertainty for the CEOP reference site at Santarem is greater than the area mean of the LBA uncertainty range by a factor of about four. Santarem is affected by the ITCZ, which contains major uncertainties related to the initial and boundary conditions (Fig. 2; see also Table 2). Another example of spatial inhomogeneity is the CEOP reference site at Sodankylä, within the BALTEX domain. The combined uncertainty range for the BALTEX domain is the second-largest of all the analyzed domains. The uncertainty range at the CEOP reference site in Sodankylä, however, has the smallest combined uncertainty range of all the CEOP reference sites (see Table 2). The uncertainty range of the initial and boundary conditions, as well as the uncertainty range involved in comparing point values with gridded data sets, are smallest at the Sodankylä site.

4. Evaluation of RSM precipitation

By estimating uncertainty ranges, model deficiencies can be identified when the difference between the simulation and observation exceeds the combined ranges of uncertainty. If deficiencies are identified, they need to be traced

Table 2. Uncertainty ranges of monthly mean precipitation [mm] at CEOP reference sites (October 2002 to March 2003).

	Initial Condition	Observation (CEOP reference site measurements)	Combined uncertainty ranges
Lindenberg	50.0	1.3	50.0
Cabauw	3.6	43.2	43.4
Sodankyla	1.8	1.2	2.2
Ft. Peck	52.0	4.8	52.2
Bondville	99.1	4.7	99.2
Oak Ridge	45.9	119.8	128.3
Mongolia	245.1	0.3	245.1
Himalayas	50.4	34.8	61.3
Pantanal	4.8	45.9	46.2
Manaus	46.2	77.1	89.9
Santarem	99.8	35.1	105.8

back to their parameterization. This is achieved by classifying the simulated precipitation into convective and stratiform precipitation.

To avoid inconsistencies related to the model boundaries, the values of the eight outer model grid boxes (sponge zone) are not taken into account in this study.

4.1 Precipitation amount

Figure 3 shows the monthly mean differences (area means) between the RSM simulation and GPCP observations for the seven domains.

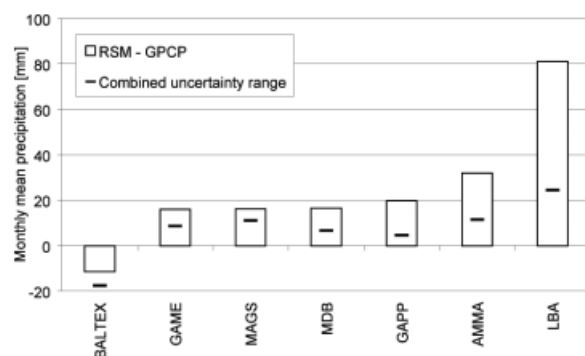


Fig. 3. Monthly mean differences (area means) of precipitation [mm] between RSM simulations and GPCP observations (monthly means for the first half of EOP III; area means).

Except for the BALTEX domain, all of the differences are positive, which means that the simulation is positively biased with respect to the GPCP observations. The positive bias is greatest for the LBA domain and smallest for the GAME domain. The black bars in Fig. 3 represent the estimated combined ranges of uncertainty for each model domain (see Table 1). Except for the BALTEX domain, the differences of all the domains exceed their estimated combined range of uncertainty. In other words, for the BALTEX domain a major component of the differences between the RSM simulation and GPCP observations is related to uncertainties in either the observations or the initial and boundary conditions, rather than resulting from biases inherent in the model. For the other domains, however, the analysis has clearly identified a bias in the model.

To further classify the characteristics of the precipitation bias, we distinguish between simulated convective and simulated stratiform/dynamic precipitation. Figure 4 shows the precipitation amount for each domain during the first half of EOP III.

Stratiform precipitation is the major component of the total precipitation over the MAGS, BALTEX, GAPP, and LBA domains, while convective precipitation is the major component of

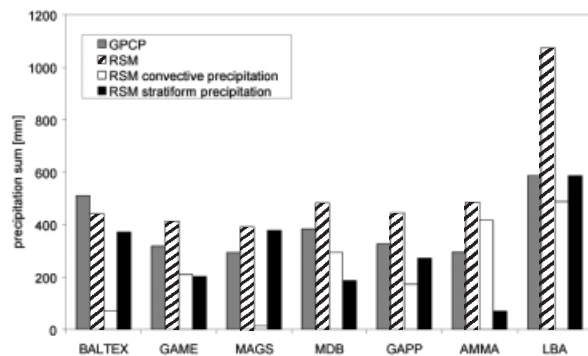


Fig. 4. Precipitation sum [mm] during the first half of EOP III (area means).

the total precipitation over the AMMA, GAME, and MDB domains. The precipitation bias over the AMMA domain is clearly related to convective precipitation, as it exceeds the total amount of observed precipitation from GPCP. For the MAGS domain, stratiform precipitation exceeds the total amount of observed precipitation from GPCP. The positive bias of the precipitation simulation in the MAGS domain can therefore be clearly assigned to stratiform precipitation. For the other domains, the source of the deficiency is not easily traced at this point, as neither convective nor stratiform precipitation alone exceeds the precipitation amount of the GPCP observations.

As mentioned above, measurements such as those undertaken at the CEOP reference site are essential in providing further information on meteorological conditions at a certain location. Global data sets lack the equivalent horizontal and temporal resolution required to provide similar information. Figure 5 shows the mean monthly precipitation differences between RSM and CEOP during the first half of EOP 3 at the CEOP reference sites.

The black bars indicate the estimated ranges of uncertainty for each CEOP reference site (see Table 2). The differences between RSM simulations and the CEOP station measurements exceed the uncertainty ranges at 4 of the 11 reference sites (Sodankylä/BALTEX, Himalayas/GAME, Pantanal/LBA, and Manaus/LBA). The largest difference occurs at Manaus, LBA, which is located in the Amazon region and is affected by the ITCZ.

Figure 6 shows the simulated convective

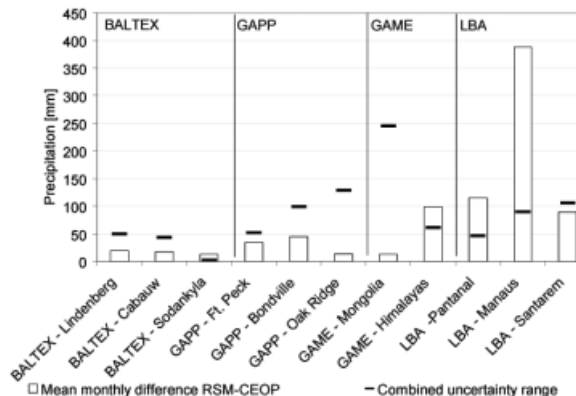


Fig. 5. Mean monthly precipitation differences [mm] between RSM simulated precipitation and CEOP precipitation measurements during the first half of EOP 3 at CEOP reference sites.

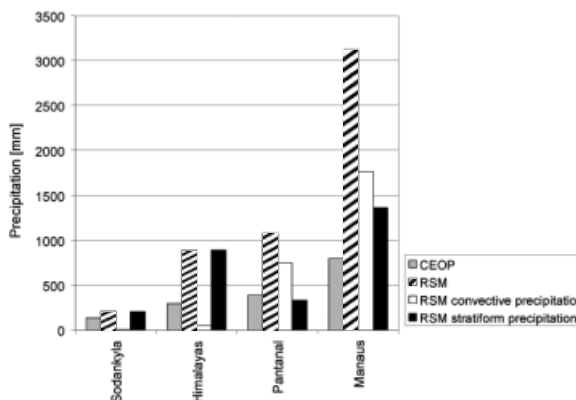


Fig. 6. Precipitation sum at those CEOP reference sites where the uncertainty range was exceeded.

and stratiform/dynamic precipitation for those CEOP reference sites for which the difference between the simulation and measurements exceeds the estimated uncertainty ranges.

At Sodankylä and Himalayas, the amount of stratiform/dynamic precipitation is greater than the measured precipitation. This means that the positive bias is related to stratiform/dynamic precipitation. At Pantanal, the amount of simulated convective precipitation is greater than the measured precipitation, which means that the positive bias at this reference site is mainly related to convective precipita-

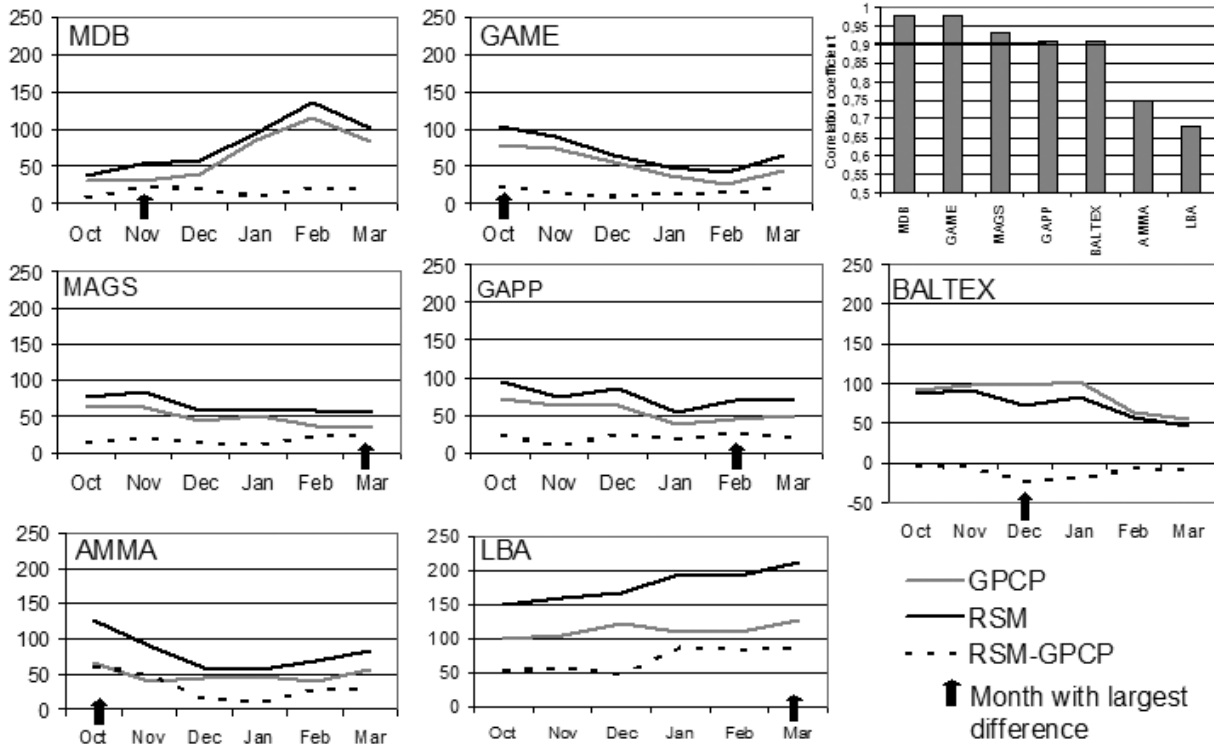


Fig. 7. Monthly precipitation sum [mm] (area means) and correlation coefficients.

tion. At Manaus, where the difference is large, both stratiform and convective precipitation have larger values than the measured precipitation amount.

4.2 Annual cycle of precipitation

Further information on the source of the precipitation biases can be derived by analyzing the annual cycle of precipitation.

Figure 7 (right-hand figure) shows the correlation coefficients (for the area averages) between RSM simulated precipitation and GPCP observed precipitation during the first half of EOP 3 for each domain. There is strong temporal correlation between the RSM simulations and GPCP observations. The correlation coefficient is above 0.9 for most domains, except for AMMA and LBA (Fig. 7, left-hand figure). MDB and GAME record the highest correlation coefficients (0.98).

Figure 8 shows the correlation coefficients for the CEOP reference sites during the first half of EOP 3.

The black columns represent the correlation coefficients between RSM and CEOP measure-

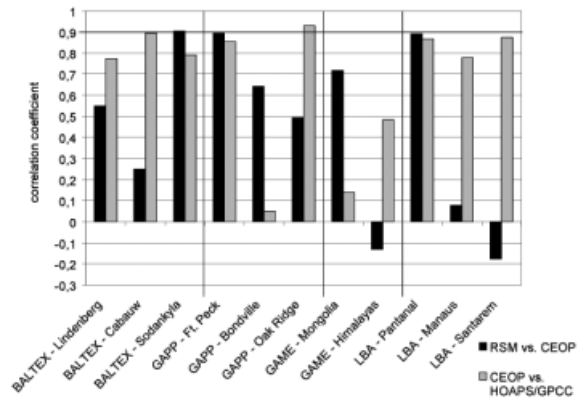


Fig. 8. Correlation coefficients of the annual cycle at CEOP reference sites for the first half of EOP 3.

ments at reference sites, while grey columns represent the correlation coefficients of CEOP reference site measurements compared with HOAPS/GPCC. The latter is an indicator of the possible correlation coefficient, taking into account the uncertainty involved in comparing point values with gridded data. Only Cabauw

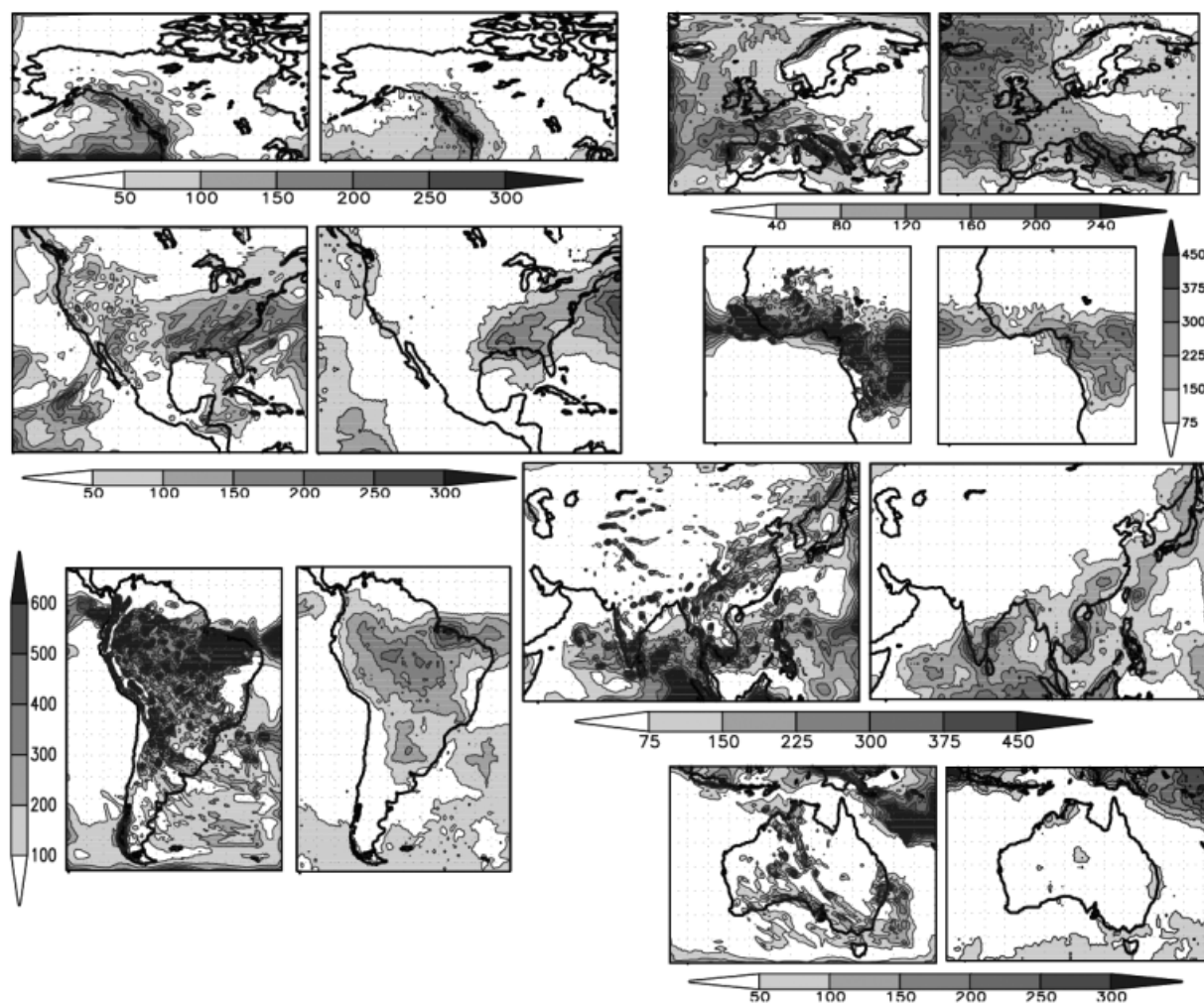


Fig. 9. Monthly precipitation sum [mm]. Left-hand figure: RSM, right-hand figure: GPCP.

and Oak Ridge show correlation coefficients in excess of 0.9. At Cabauw, Lindenberg, Oak Ridge, Himalayas, Manaus, and Santarem, the correlation coefficients of CEOP vs. HOAPS/GPCP are larger than those of RSM vs. CEOP. This means that the simulated annual cycle at these locations might be deficient. Based on the locations of these CEOP reference sites, we speculate that this deficiency in the simulation of the annual cycle might be associated with westerly winds, the ITCZ, or the northeast Monsoon in Southeast Asia.

4.3 Spatial distribution of precipitation

For each domain, the month with the greatest difference between the RSM and GPCP (see

Fig. 7, left-hand figure, black arrows) was selected to analyze the spatial structure of the precipitation. The greatest differences were recorded in December 2002 for the BALTEX domain, February 2003 for the GAPP domain, March 2003 for the LBA and MAGS domains, October 2003 for the GAME and AMMA domains, and November 2002 for the MDB domain.

Figure 9 shows the spatial distribution of the sum of monthly precipitation for the selected months.

For every domain, the RSM simulated precipitation is shown on the left and the GPCP observed precipitation is shown on the right. The RSM is clearly capable of simulating the

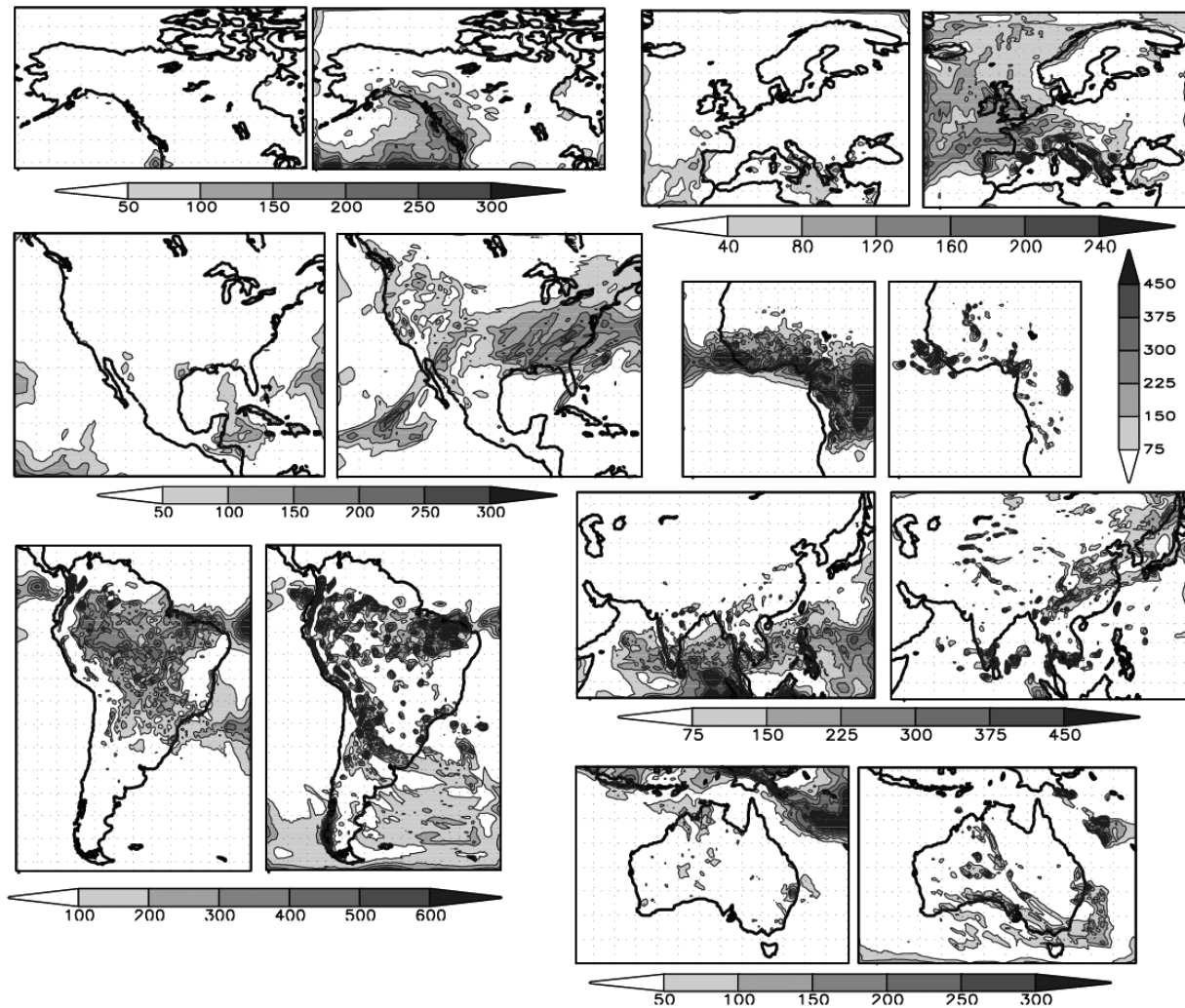


Fig. 10. Mean monthly precipitation sum [mm]. Left-hand figure: convective, right-hand figure, stratiform.

correct spatial distribution of precipitation. The positive bias for precipitation occurs in regions where the GPCP data set records the greatest amount of precipitation. The ITCZ has the greatest impact on precipitation in the LBA and AMMA domains. The greatest differences between the RSM and GPCP in these domains are associated with the ITCZ. Over the BALTEX domain, precipitation has a negative bias over Scandinavia and over the Atlantic Ocean. Over areas of elevated topography, however, the precipitation bias is positive. These impacts recorded over the BALTEX domain are not dominant in terms of the meteorological conditions of the domain, and the estimated un-

certainty range is not exceeded by the difference between the RSM simulated precipitation and GPCP precipitation.

To obtain further insight into the source of the precipitation bias, the RSM simulated precipitation was again separated into convective and stratiform precipitation. For the same months as those shown in Fig. 9, Fig. 10 shows the monthly total convective (left-hand figure) and stratiform (right-hand figure) precipitation for each domain.

Figure 10 shows that convective precipitation associated with the ITCZ constitutes the bulk of the source of the positive bias. This is true for AMMA, the area over the Amazon in the

LBA domain, and the area southwest of New Guinea in the MDB domain. An additional source of the positive bias for convective precipitation is the northeast Monsoon in Southeast Asia, especially over the Gulf of Bengal and the Pacific Ocean within the GAME domain.

A positive bias is also associated with stratiform precipitation over elevated topography and the forced lifting of air masses over mountainous regions. These features occur in the GAPP domain where air masses are moved by westerly winds over the Rocky Mountains and the Appalachians. In the GAME domain, air masses of the northeast monsoon are lifted over the mountains of Central Asia (Kunlun Mountains, Himalayas, Altay Mountains), and at the coast of the Sea of Japan the air mass is lifted over the Skhote Alin Mountains. In the LBA domain, excessive stratiform/dynamic precipitation occurs where the trade winds move air masses over the northeast Brazilian Highlands and the Andes, and in the MAGS domain the stratiform/dynamic bias occurs where the westerlies move air masses over the Coast Mountains. The BALTEX domain shows this phenomenon at smaller scales, with the so-called foehn effect observed over the Alps, Pyrenees, and Apennine Mountains.

5. Sensitivity tests with four different convection schemes

In addition to the default Relaxed Arakawa–Scheme (RAS) (Moorthi and Suarez, 1992) used for the initial comparison, we also examined the following schemes:

- 1) Simplified Arakawa Scheme (SAS), (Pan and Wu 1995);
- 2) Kain–Fritsch scheme (KF), (Kain and Fritsch 1993); and
- 3) National Centers for Atmospheric Research (NCAR) Community Climate Model (CCM) scheme (Zhang and McFarlane 1995).

The four convection schemes introduced above can be largely characterized as: 1) those schemes based on the Arakawa–Schubert scheme (RAS, SAS, and NCAR/CCM), and 2) the Kain–Fritsch scheme. The Arakawa–Schubert scheme was developed with consideration of the Global Atmospheric Research Program Atlantic Tropical Experiment (GATE) ocean-based data set, whereas the Kain–Fritsch scheme was intended for land-based convection. A summary of the strengths and limitations of these schemes can be found in Appendix II.

For each model domain (see Fig. 1 and Section 2.3), test runs were carried out using these four convection schemes for the month that recorded the greatest differences between RSM simulated precipitation and GPCP observed precipitation (see Fig. 7, left-hand figure, black arrows). Table 3 shows the uncertainty ranges for the test months, and Fig. 11 shows the differences between the RSM using the four different convection schemes and GPCP data.

The black bars in Fig. 11 indicate the uncertainty ranges (area means) for each domain. To ensure that the RAS convection schemes were comparable in terms of the spin up time, the RSM was run a second time using the RAS convection scheme for the respective selected

Table 3. Uncertainty ranges for the test months [mm/month] (area averages)

	Selected Month	Initial condition	Observation	Combined uncertainty range
AMMA	10/02	3.4	9.1	9.7
BALTEX	12/02	16.5	24.5	29.5
GAME	10/02	7.4	11.4	13.6
GAPP	02/03	9.6	0	9.6
LBA	03/03	35.7	32.1	48
MAGS	03/03	5.2	3.8	6.4
MDB	11/02	9.2	6.2	11.1

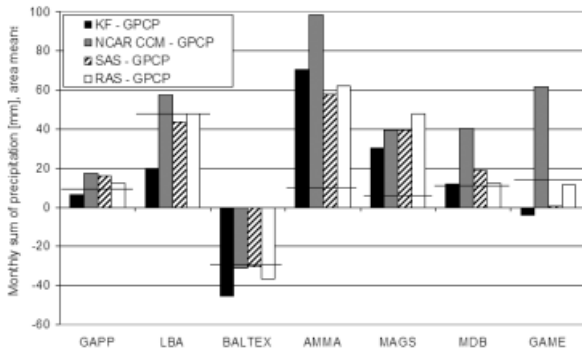


Fig. 11. Differences (area means) in monthly mean precipitation [mm] between RSM with different convection schemes minus GPCP (area means during the test months).

months for each domain. For each domain, at least one convection scheme resulted in smaller biases than the RAS convection scheme. When using the particular convection schemes that produced the smallest bias, some of the differ-

ences between the RSM test runs and GPCP no longer exceed the uncertainty range. The smallest mean biases occurred for the LBA, MDB, MAGS, and GAPP domains using the KF scheme, and for the BALTEX, AMMA, and GAME domains using the SAS scheme. Depending on the spatial distribution of precipitation, a certain convection scheme can be recommended for a particular domain for extended simulations.

Figure 12 shows the spatial distribution of precipitation over the GAPP domain.

In this case, all of the convection schemes have similar deficiencies, including a positive bias over the Caribbean, the Rocky Mountains, and the Appalachians. As deduced from Fig. 10, the overestimation over the Rocky Mountains and the Appalachians is mainly caused by stratiform precipitation. The precipitation amount, however, is also related to the respective convection scheme. As already demonstrated by the area means of the differences in Fig. 11, the smallest differences between RSM and GPCP data occur when the KF convection

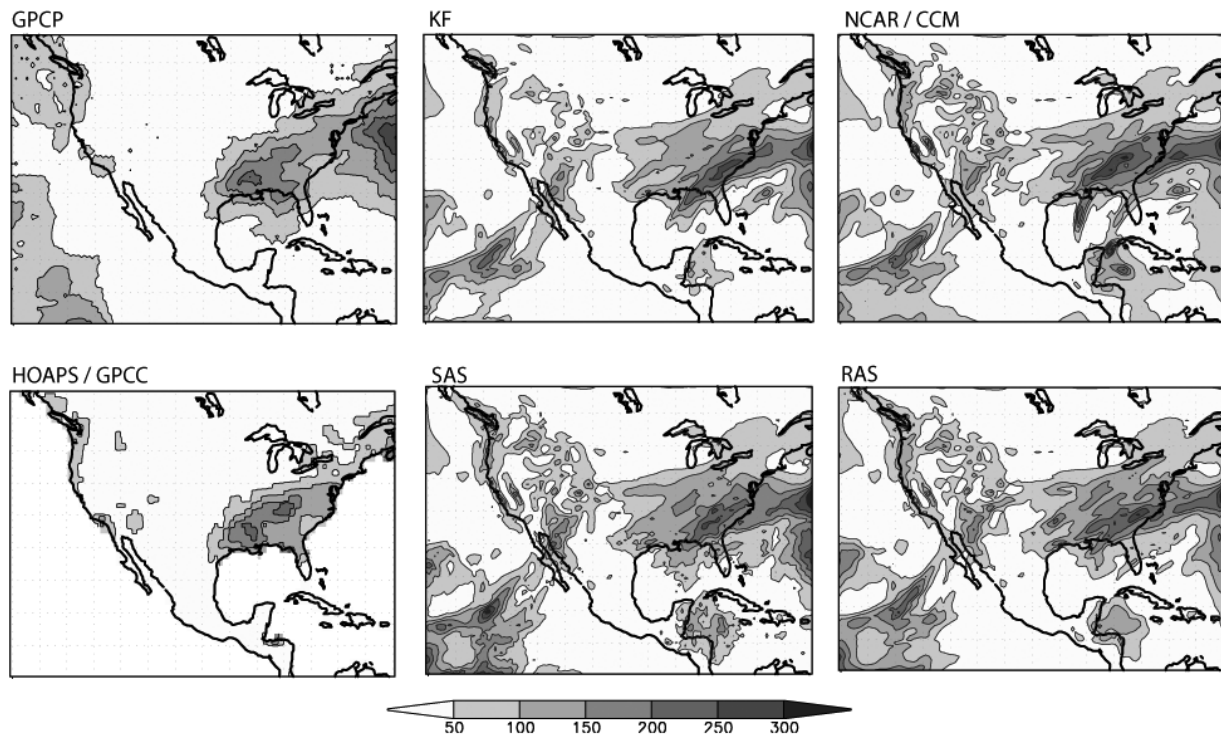


Fig. 12. Precipitation sum over GAPP for the test months, as derived from GPCP and HOAPS/GPCC data and from RSM simulations using four different convection schemes.

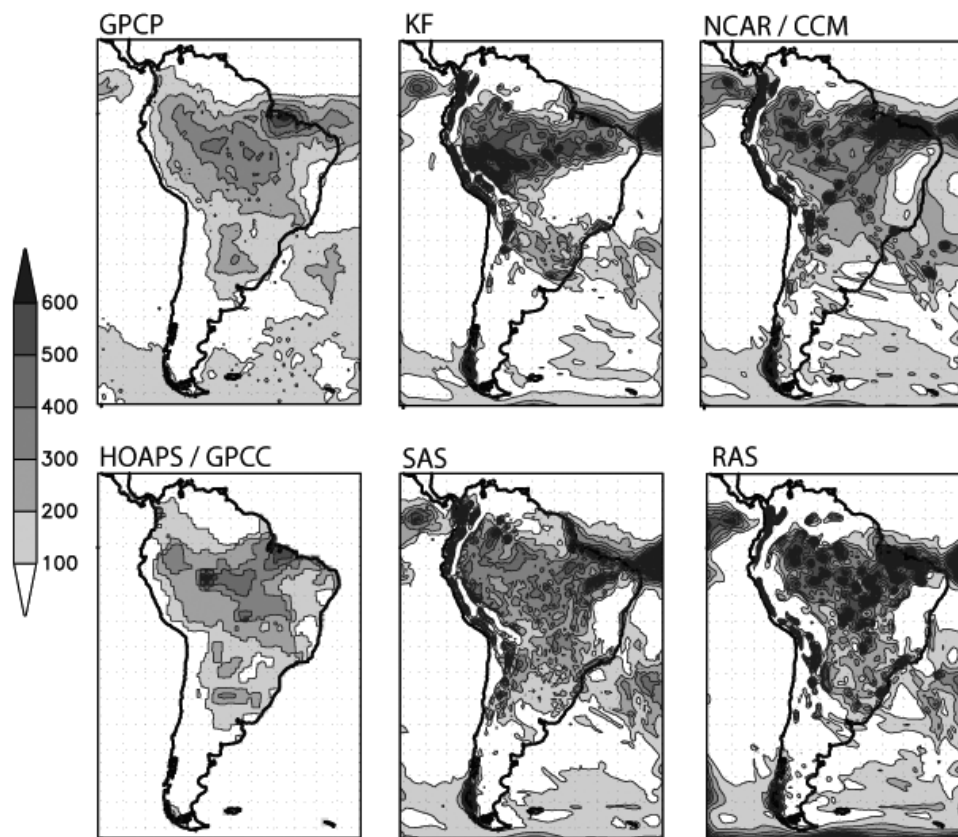


Fig. 13. Precipitation sum [mm] over LBA for the test months, as derived from GPCP and HOAPS/GPCC data and from RSM simulations using four different convection schemes.

scheme is used. This simulation has the smallest positive bias over the Rocky Mountains, the Appalachians, and the Caribbean, and the area mean difference between RSM with the KF scheme and GPCP does not exceed the range of uncertainty. The KF scheme is therefore recommended as the default convection scheme over the GAPP domain.

Figure 13 shows the spatial distribution of precipitation over the LBA during the test month.

As shown in Fig. 11, the biases of the KF and SAS convection schemes do not exceed the uncertainty range. Although the precipitation area mean produced when using the KF scheme shows the smallest difference when compared with GPCP data (see Fig. 11), the spatial distribution of the KF scheme is not the best of the convection schemes. All convection schemes have major problems in simulat-

ing precipitation associated with the ITCZ, and the KF scheme records the largest differences with GPCP data within the ITCZ. Over the Brazilian Highlands, however, precipitation has a negative bias, resulting in a small area average even though the predicted spatial distribution of precipitation is less accurate than that of the other convection schemes. The spatial distribution of precipitation simulated by the SAS convection scheme is most similar to the observed precipitation, as the precipitation bias related to the ITCZ is the smallest of the tested schemes. The SAS convection scheme is therefore recommended as the default convection scheme for the LBA domain. As we are unable to reach a conclusion regarding the annual cycle on the basis of a 1-month test run, further analyses are required with long-term runs and different convection schemes.

Figure 14 shows the spatial distribution of

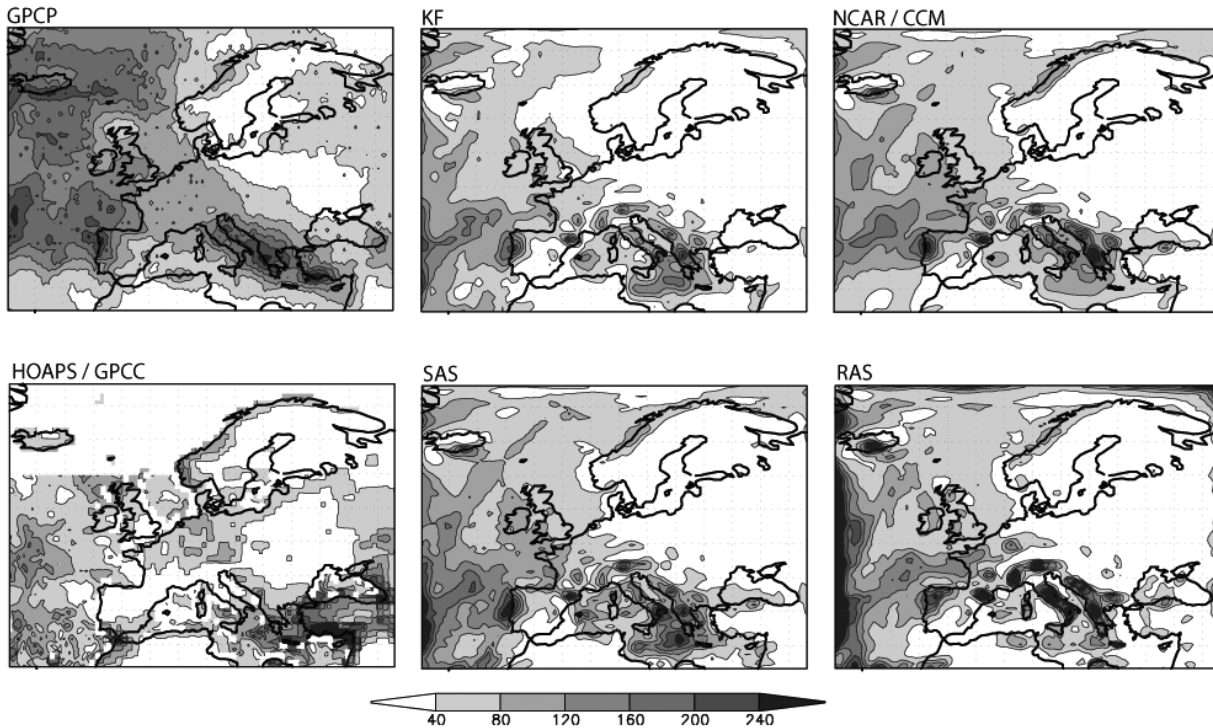


Fig. 14. Precipitation sum [mm] over BALTEX for the test months, as derived from GPCP and HOAPS/GPCC data and from RSM simulations using four different convection schemes.

the monthly sum of precipitation over the BALTEX domain.

As shown in Fig. 11, the area mean difference between RSM_SAS and GPCP is the smallest of all the domains. The SAS convection scheme most closely resembles the spatial distribution of the GPCP observed precipitation, and is thus recommended for the BALTEX region. Although the difference between RSM_SAS and GPCP (0.5 mm) is slightly above the uncertainty range, previous results (see Section 4.1 and Fig. 3) demonstrate that precipitation in the BALTEX domain is unbiased for longer simulation periods when the surface model is equilibrated. This means that equilibration of the surface water may eventually be essential for a full evaluation of convective parameterizations, at least for some of the domains.

The spatial distribution of precipitation in the AMMA domain is shown in Fig. 15.

As shown in Fig. 11, none of the four convection schemes were able to reduce the difference between RSM simulated precipitation and GPCP data below the uncertainty range. The

sole source of these differences is precipitation associated with the ITCZ. The smallest differences in the area means were achieved using the SAS convection scheme. This is also true for the spatial distribution of precipitation (Fig. 15), where SAS produced the best simulation results. The SAS convection scheme is therefore recommended as the default convection scheme for the AMMA domain. Further investigations are required, however, as the ITCZ and its annual cycle continue to remain a major problem for all parameterizations.

Figure 16 shows the spatial distribution of the precipitation sum over the MAGS domain.

In the test runs, all of the convection schemes show a positive precipitation bias over land and in the northern part of the domain. In the long term run these biases did not exist. Again, this indicates that equilibration of the surface water may eventually be essential for a full evaluation of convective parameterizations. Other regions with a positive bias are those over the Coast Mountains and the Gulf of Alaska. As determined from Fig. 10, this positive bias

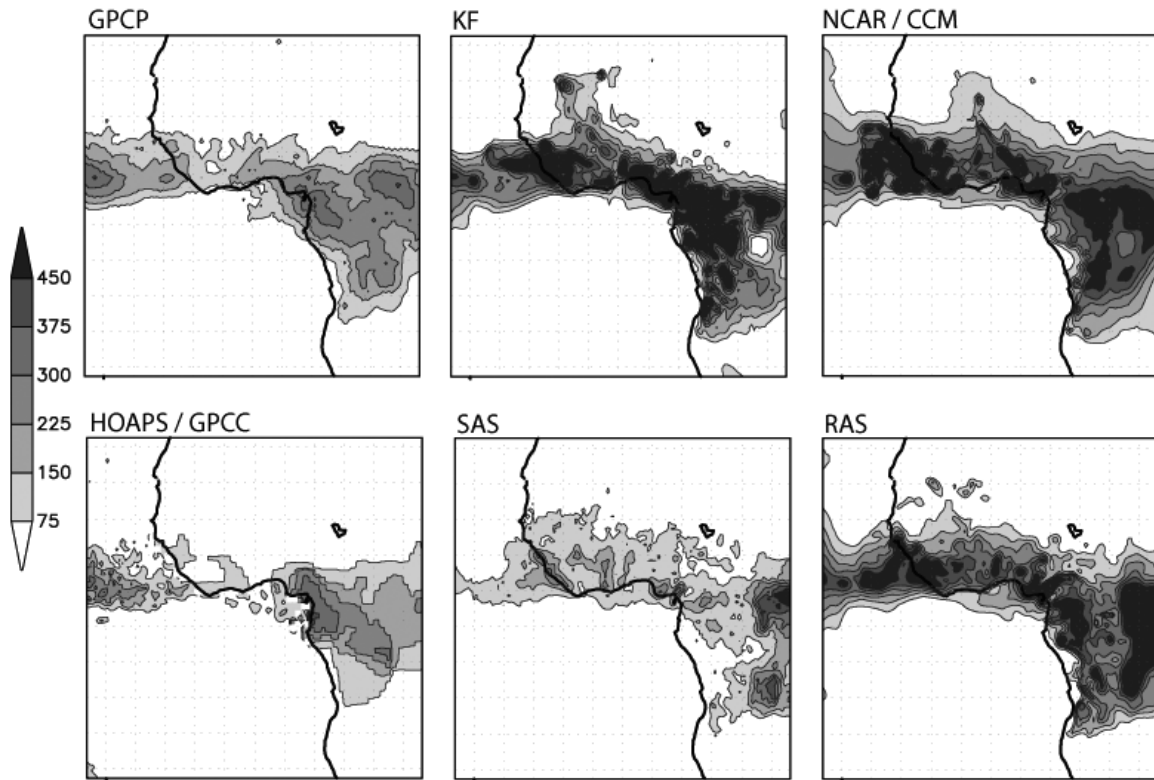


Fig. 15. Precipitation sum [mm] over AMMA for the test months, as derived from GPCC and HOAPS/GPCP data and from RSM simulations using four different convection schemes.

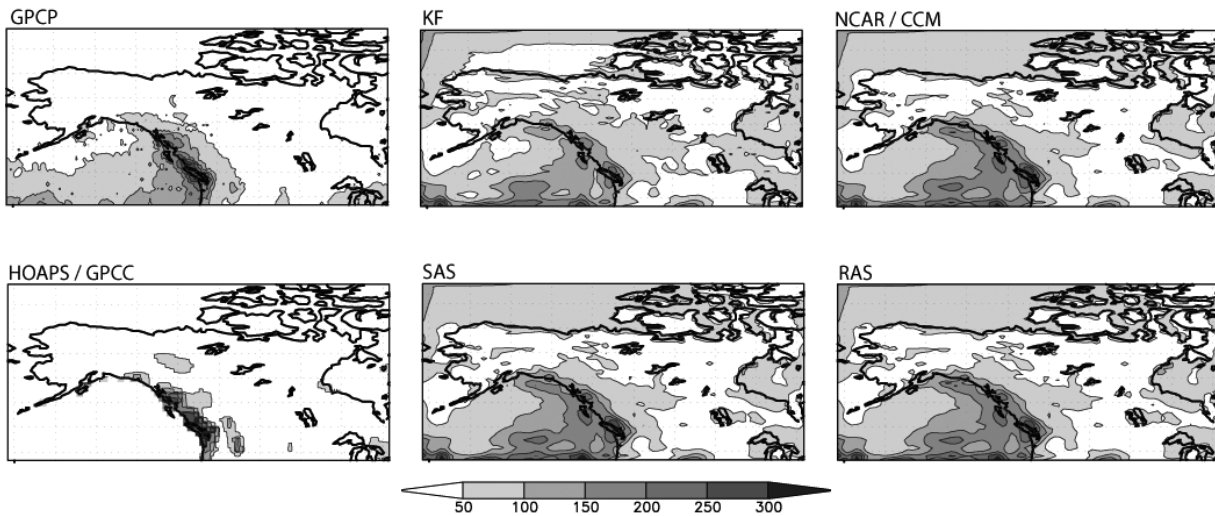


Fig. 16. Precipitation sum [mm] over MAGS for the test months, as derived from GPCP and HOAPS/GPCC data and from RSM simulations using with four different convection schemes.

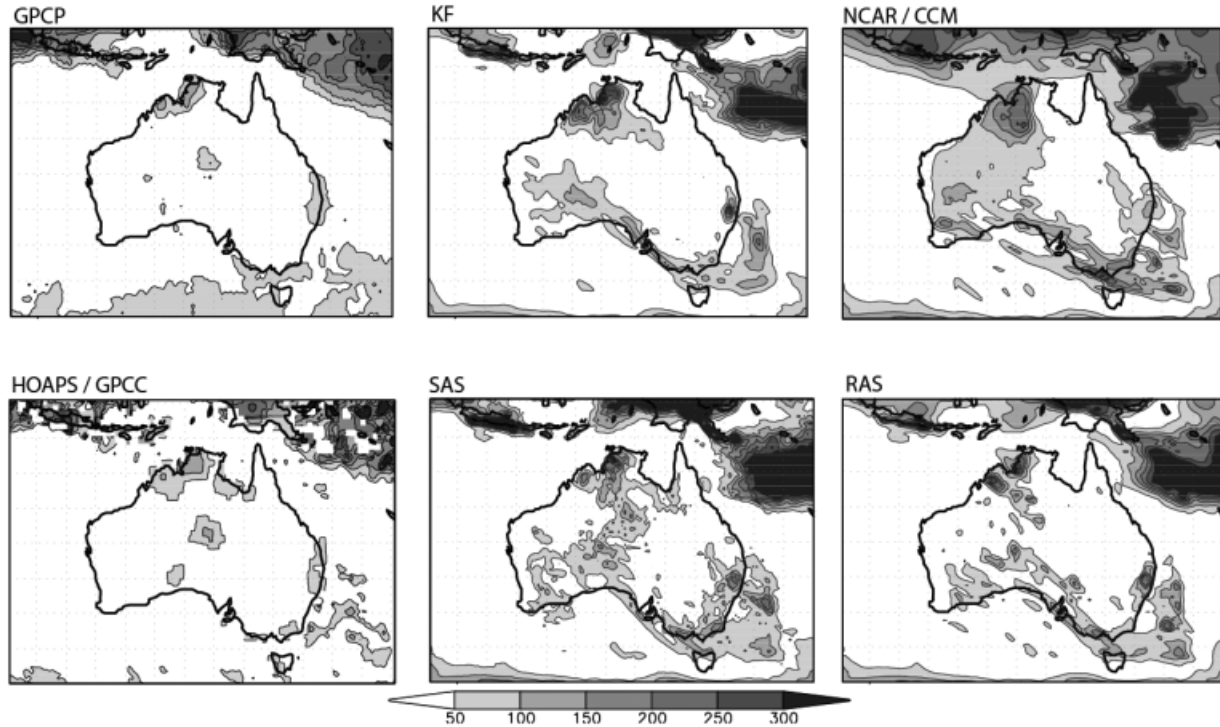


Fig. 17. Precipitation sum [mm] over MDB for the test months, as derived from GPCP and HOAPS/GPCC data and from RSM simulations using four different convection schemes.

is mainly the result of stratiform precipitation. The precipitation amount, however, is also related to the respective convection schemes. This bias is smallest when using the KF scheme, making this the recommended scheme for the prediction of precipitation in the MAGS domain. As the difference between the RSM with KF scheme and GPCP still exceeds the uncertainty range, it is important to undertake additional analyses of stratiform precipitation in the MAGS domain.

Figure 17 shows the spatial distribution of precipitation over the MDB domain.

The major component of the positive bias for all test runs is associated with the ITCZ (New Guinea and the area southeast of New Guinea). The KF scheme results in the smallest mean bias and the smallest bias associated with the ITCZ. This scheme is therefore recommended for simulations of precipitation in the MDB domain. The difference between the RSM with KF scheme and GPCP still slightly exceeds the uncertainty range (0.7 mm). As already shown for the AMMA and LBA domains, the precipitation

bias associated with the ITCZ is the major source of this difference. Further parameterization improvements are therefore required for tropical convection.

For the GAME domain, the RAS, SAS, and KF convection schemes have area mean differences (RSM minus GPCP) below the uncertainty range (Fig. 11). The area mean difference is smallest between the RSM with SAS scheme and the GPCP observations (Fig. 11), and the spatial distribution of simulated precipitation is closest to the observed data when the SAS convection scheme is used (Fig. 18).

The SAS convection scheme is therefore recommended for the simulation of RSM precipitation over the GAME domain. Table 4 provides a summary of the above results for each domain.

6. Discussion and conclusions

Our comparison of simulated and observed precipitation highlights the following crucial requirements that are valuable for any evaluation of simulated precipitation. 1) The comparisons are carried out over regions with con-

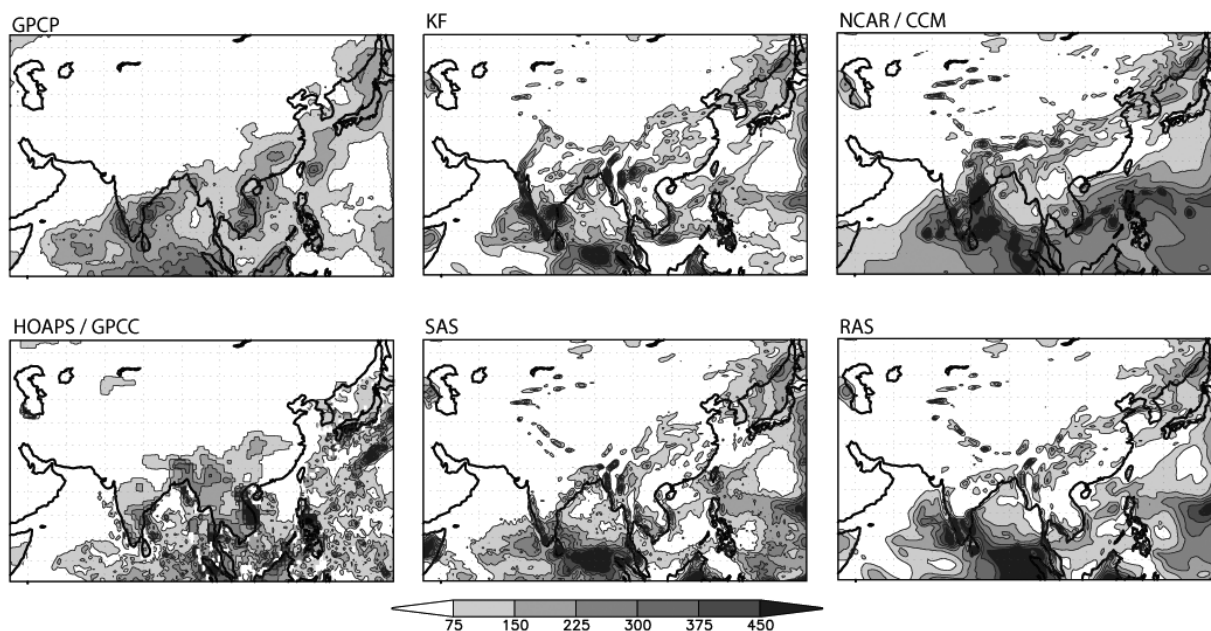


Fig. 18. Precipitation sum [mm] over GAME for the test months, as derived from GPCP and HOAP/GPCC data and from RSM simulations using four different convection schemes.

Table 4. Results of the sensitivity studies with four different convection schemes

	Convection scheme recommended	Focus of further analyses
GAPP	Kain Fritsch Scheme	None
MAGS	Kain Fritsch Scheme	Stratiform precipitation, equilibration of the surface model is essential
MDB	Kain Fritsch Scheme	ITCZ processes
BALTEX	Simplified Arakawa Schubert Scheme	None, however equilibration of the surface model is essential
GAME	Simplified Arakawa Schubert Scheme	None
AMMA	Simplified Arakawa Schubert Scheme	ITCZ processes, annual cycle
LBA	Simplified Arakawa Schubert Scheme	Annual cycle

trasting physical and dynamical meteorological conditions. 2) Uncertainty ranges are estimated using the concept of confidence bands. For this purpose, equivalent but random realizations of the process that generates the data (i.e., simulations and observations) are needed to ensure the accurate estimation of the uncertainty range. In the present study, we ensured that we possessed two realizations of the simulated and observed precipitation available for

the analyses. This strategy provided a rapid method of comparing our model results with observational data. 3) Once a model bias has been identified, possible sources for the biases are classified, where possible, as either convective or stratiform.

In summary, RSM precipitation provides a reasonable estimate of seasonal variations in precipitation and spatial patterns of precipitation; however, a positive bias in the RSM

simulation of precipitation amount was found over most regions. The bias is associated with ITCZ convection, monsoonal convection, and the forced lifting of air masses over elevated topography. The exception is the BALTEX domain, which does not show a significant domain averaged bias.

The most appropriate convection scheme for each domain, which acted to reduce the positive bias and increase the accuracy of the model simulations was identified via sensitivity tests conducted using four different convection schemes. The sensitivity tests reveal that the biases for most of the precipitation simulations can be improved for all domains by using either the KF scheme or the SAS scheme. The greatest improvement in terms of modeling results for the ITCZ and monsoonal convective precipitation is obtained by using the SAS convection scheme. The SAS convection scheme is recommended for AMMA, BALTEX, GAME, and LBA, while the KF convection scheme is recommended for GAPP, MAGS, and MDB. Further improvements in the parameterization of rainfall are required for the ITCZ and its annual cycle as well as precipitation associated with the forced lifting of air masses.

The dependence of the accuracy of the precipitation simulations on the different convective schemes demonstrates there are currently no universal convective parameterizations that apply to all geographical locations and meteorological situations. This indicates that global models that currently use a single parameterization scheme can be further improved by the development of universally applicable convective parameterizations. Another possibility might be to use different parameterizations for different regions or situations, as identified in this study. Identifying and understanding the conditions and reasons behind the optimal performance of different convection schemes might prove to be useful in developing a more universally applicable convective parameterization.

Acknowledgements

This study was supported by NOAA NA17RJ1231 and NASA NNG06GC85G. The views expressed herein are those of the authors and do not necessarily reflect the views of NOAA or NASA. Comments by anonymous re-

viewers were helpful in improving the presentation of the results.

Appendix I

Uncertainties in the simulations and observations

The uncertainty range for both factors in each domain is estimated by applying the concept of confidence bands (e.g., von Storch and Zwiers 1999). To formalize this, the random variable (\mathbf{W}) is introduced. When there are n samples W_i of \mathbf{W} , the mean value is estimated using

$$\mu = \frac{1}{n} \sum_{i=1}^n W_i$$

and the variance is estimated using

$$\sigma_w^2 = \frac{1}{n} \sum_{i=1}^n (W_i - \mu)^2.$$

The α confidence interval, which on average contains α of all realizations W_i of \mathbf{W} , is given by

$$P(W \in [\mu - k\sigma_w; \mu + k\sigma_w]) = \alpha \quad \text{with} \\ k = S^{-1}\left(\frac{\alpha + 1}{2}\right),$$

where S represents the distribution function of the normal distribution and P is the probability of the event given in parentheses. Thus, $\pm S^{-1}\left(\frac{\alpha + 1}{2}\right)\sigma_w$ is the uncertainty at a given level of α . Thus, if $\alpha = 95\%$, then $k = S^{-1}(0.975)$ and the uncertainty is $\pm 1.96\sigma_w$. The greater the number of available realizations of simulations and observations, the greater the precision of the estimated uncertainty ranges. The problem of estimating the unknown parameters μ and σ_w when few data are available is discussed in Meinke (2006) and Meinke et al. (2004). At least two realizations of both the simulations and observations are required; these are denoted as W_1 and W_2 . Then,

$$\mu = [W_1 + W_2]/2 \quad \text{and} \\ \sigma_w^2 = \frac{1}{2}([W_1 - \mu]^2 + [W_2 - \mu]^2) \\ \sigma_w^2 = [W_1 - W_2]^2/4.$$

The level of $\alpha = 95\%$ is used in the calculation of all of the uncertainty ranges. The combined range of uncertainties (U) generated by the model ($k\sigma_{w(\text{MODEL})}$) and the precipitation observation ($k\sigma_{w(\text{OBS})}$) is given by

$$U = \sqrt{(k\sigma_{w(\text{MODEL})}^2 + k\sigma_{w(\text{OBS})}^2)}.$$

Although this provides only a crude estimation of the uncertainty range, this is very useful for evaluation of the model and it helps to distinguish between actual model deficiencies and uncertainties.

Appendix II

Strengths and limitations of the two main convection schemes

	Strengths	Limitations
Arakawa–Schubert scheme	<p>Accounts for the influences of entrainment, detrainment, and compensating subsidence around clouds.</p> <p>Can account for Convective Available Potential Energy (CAPE), depending on the specific implementation details.</p> <p>Some implementations can account for saturated and/or unsaturated downdrafts, tilting of updrafts such that rain falls through cloud or is ejected outside the tower, and/or microphysical processes that occur during convection.</p> <p>Complex scheme that deals with a variety of cloud depths and is capable of providing complex sounding changes that correspond to many different forecast situations.</p>	<p>May not sufficiently stabilize the model atmosphere.</p> <p>May produce rain that is delayed relative to the observed data or result in a prolonged period of weak convection.</p> <p>May result in grid-scale convection. This leads to many negative forecast impacts, including changes to the model's mass fields.</p> <p>The scheme is not designed for elevated convection.</p> <p>Assumes that convection exists over only a very small fraction of the grid column; this may not be appropriate for higher-resolution models.</p> <p>Assumes that convective updrafts entrain through the sides of the cloud, whereas observations of cumulus and towering cumulus indicate entrainment mainly through the cloud top. This affects scheme rainfall and heating profiles, which feed back into the resolved motions.</p>
Kain–Fritsch Scheme	<p>Suitable for mesoscale models and coupling with parameterization schemes that use clouds.</p> <p>The assumption concerning the consumption of CAPE is appropriate for short time-scales and small spatial scales.</p> <p>The scheme accounts for microphysical processes in convection; it can be set up to feed hydrometeors to the parameterization scheme.</p> <p>May yield superior performance in cases of severe convection.</p> <p>Physically realistic in many ways.</p> <p>Accounts for entrainment and detrainment more realistically than Arakawa–Schubert schemes.</p> <p>Takes account of elevated convection.</p> <p>Able to vary its response to different forecast scenarios.</p>	<p>Tends to generate unrealistically deep saturated layers in post-convective soundings (the parameterization scheme will then activate, simulating post-convective stratiform precipitation that may be overestimated).</p> <p>Assumption of the rapid consumption of CAPE is inappropriate for coarse-resolution models such as climate models.</p> <p>Model fields may appear “splotchy” because of convection that is triggering in scattered grid boxes (other schemes tend to produce a smoother clustering of grid boxes where convection is triggered). Although this approach may be more realistic, it can hinder the interpretation of model fields.</p>

(Kuo et al. 1996, Wang and Seaman 1997, Arakawa and Schubert 1974, Kain and Fritsch 1992)

References

- Adler, R.F., G.J. Huffman, A. Chang, R. Ferraro, P. Xie, J. Janowiak, B. Rudolf, U. Schneider, S. Curtis, D. Bolvin, A. Gruber, J. Susskind, P. Arkin, and E. Nelkin, 2003: The version-2 global precipitation climatology project (GPCP) monthly precipitation analysis (1979–present), *J. Hydrometeorol.*, **4**, 1147–1167.
- Anderson, B.T., J.O. Roads, S.-C. Chen, and H.-M.H. Juang, 2000a: Regional Simulation of the Low-level Monsoon Winds over the Gulf of California and Southwest United States. *JGR-Atmospheres*, **105**, 17955–17969.
- Anderson, B.T., J.O. Roads, and S.-C. Chen, 2000b: Large-scale Forcing of Summertime Monsoon Surges Over the Gulf of California and Southwest United States. *JGR-Atmospheres*, **105**, 455–467.
- Anderson, B.T., J.O. Roads, S.-C. Chen, and H.-M.H. Juang, 2001: Model Dynamics of Summertime Low-Level Jets over Northwest Mexico. *JGR-Atmospheres*, **106**, 3401–3413.
- Anderson, B.T. and J.O. Roads, 2002: Regional Simulation of Summertime Precipitation over the Southwestern United States. *J. Climate*, **15**, 3321–3342.
- Arakawa, A. and W.H. Schubert, 1974: Interaction of a cumulus cloud ensemble with the large-scale environment, Part I. *J. Atmos. Sci.*, **31**, 674–701.
- Bauer, P. and P. Schlüssel, 1993: Rainfall, Total Water, Ice Water, and Water Vapor Over Sea From Polarized Microwave Simulations and Special Sensor Microwave/Imager Data. *J. Geophys. Res.*, **98**, 20737–20759.
- Buizza, R., 2000: Chaos and weather prediction. ECMWF Int. Rep. 01/2000, 41 pp.
- Chen, S.-C., J.O. Roads, H.-M.H. Juang, and M. Kanamitsu, 1999: Global to regional simulation of California's wintertime precipitation. *J. Geophys. Res.*, **104**, 31517–31532.
- Christensen, H.J. (Coordinator), 2005: PRUDENCE: Prediction of Regional scenarios and Uncertainties for defining European climate Change risks and Effects. Final Report, pp. 269.
- Christensen, J.H., T.R. Carter, and M. Rummukainen, 2006: Evaluating the performance and utility of regional climate models: the PRUDENCE project. *Climatic Change*. Accepted for publication.
- Grassl, H., V. Jost, R. Kumar, J. Schulz, P. Bauer, and P. Schlüssel, 2000: The Hamburg Ocean-Atmosphere Parameters and Fluxes from Satellite Data (HOAPS): A Climatological Atlas of Satellite-Derived Air-Sea-Interaction Parameters over the Oceans, Report No. 312, ISSN 0937-1060, Max Planck Institute for Meteorology, Hamburg.
- Han, J. and J. Roads, 2004: US Climate Sensitivity Simulated with the NCEP Regional Spectral Model. *Climate Change*, (in press).
- Hong, S.-Y. and A. Leetmaa, 1999: An evaluation of the NCEP RSM for regional climate modeling. *J. Climate*, **12**, 592–609.
- Huffman, G.J., R.F. Adler, P. Arkin, A. Chang, R. Ferraro, A. Gruber, J. Janowiak, A. McNab, B. Rudolf, and U. Schneider, 1997: The global precipitation climatology project (GPCP) combined precipitation dataset, *Bull. Amer. Meteor. Soc.*, **78**, 5–20.
- Juang, H. and M. Kanamitsu, 1994: The NMC nested regional spectral model. *Mon. Wea. Rev.*, **122**, 3–26.
- Juang, H., S. Hong, and M. Kanamitsu, 1997: The NMC nested regional spectral model. An update. *Bull. Amer. Meteor. Soc.*, **78**, 2125–2143.
- Kalnay, E. and coauthors, 1996: The NCEP/NCAR 40-Year Reanalysis Project. *Bull. Amer. Meteor. Soc.*, **77**, 437–471.
- Kain, J. and J.M. Fritsch, 1993: Convective parameterization for mesoscale models: The Kain-Fritsch scheme. The Representation of Cumulus Convection in Numerical Models, Meteor. Monograph No. 46, Amer. Meteor. Soc., Boston, 165–170.
- Kanamitsu, M., W. Ebisuzaki, J. Woolen, J. Potter, and M. Fiorino, 2002: NCEP/DOE AMIP-II Reanalysis (R-2). *Bull. Amer. Meteor. Soc.*, **83**, 1631–1643.
- Kuo, Y.-H., R.J. Reed, and Y. Liu, 1996: The ERICA IOP 5 storm. Part III: Mesoscale cyclogenesis and precipitation parameterization. *Mon. Wea. Rev.*, **124**, 1409–1434.
- Meinke, I., H. von Storch, and F. Feser, 2004: A validation of the cloud parameterization in the regional model SN-REMO, *J. Geophys. Res.*, **109**, D13205, doi:10.1029/2004JD004520.
- Meinke, I., 2006: A comparison of simulated clouds to ISCCP data, *Mon. Wea. Rev.* **134**, No. 6, pp 1669–1681.
- Mearns, L.O., F. Giorgi, L. McDaniel, and C. Shields, 1995: Analysis of daily variability of precipitation in a nested regional climate model: comparison with observations and doubled CO₂ results, *Global Planet. Change*, **10**, 55–78.
- Moorthi, S. and M.J. Suarez, 1992: Relaxed Arakawa-Schubert: A parameterization of moist convection for general circulation models. *Mon. Wea. Rev.*, **120**, 978–1002.
- Osborn, T.J. and M. Hulme, 1998: Evaluation of the European daily precipitation characteristics from the Atmospheric Model Intercomparison Project. *Int. J. Climatology*, **18**, 505–523.

- Roads, J.O., S. Chen, M. Kanamitsu, and H. Juang, 1999: Surface water characteristics in NCEP global spectral model reanalysis. *J. Geophys. Res.*, **104**, 19,307–19,327.
- Roads, J.O. and S.-C. Chen, 2000: Surface Water and Energy Budgets in the NCEP Regional Spectral Model. *JGR-Atmospheres*, **105**, 29539–29550.
- Roads, J., S. Chen, L. Druyan, M. Fulakeza, S. Cocks, T. LaRow, J.-H. Qian, and S. Zebiak, 2003a: International Research Institute/Applied Research Centers (IRI/ARCs) regional model intercomparison over South America. *J. Geophys. Res.*, **108**, doi:10.1029/2002JD003201.
- Roads, J., S.-C. Chen, and M. Kanamitsu, 2003b: US Regional Climate Simulations and Seasonal Forecasts. *JGR-Atmospheres*, **108**, doi:10.1029/2002JD002232.
- Roads, J. and coauthors, 2003c: GCIP Water and Energy Budget Synthesis (WEBS). *J. Geophys. Res.*, **108**, doi:10.1029/2002JD002583.
- Roads, J.O., 2004a: Experimental Weekly to Seasonal, Global to Regional US Precipitation Forecasts. *J. Hydrology-Special issue: Quantitative Precipitation Forecasting II*, **288** (1–2), 153–169. doi:10.1016/j.jhydrol.2003.11.033.
- Roads, J., 2004b: Experimental Weekly to Seasonal U.S. Forecasts with the Regional Spectral Model, *Bulletin of the American Meteorological Society* **85**(12) Dec 2004. 1887–1902.
- Rockel, B., I. Meinke, J. Roads, W.J. Gutowski, Jr., R.W. Arritt, E.S. Takle, and Jones, 2005: The Inter-CSE Transferability Study CEOP Newsletter 2005 (available at: <http://www.ceop.net>).
- Palmer, T.N., 2000: Predicting uncertainty in forecasts and climate. In: *Rep. Prog. Phys.*, **63**, 71–116.
- Pan, H.-L. and W.-S. Wu, 1995: Implementing a mass flux convection parameterization package for the NMC medium-range forecast model. NMC Office Note 409, 40 pp. [Available from NCEP/EMC, 5200 Auth Rd., Camp Springs, MD 20746.
- Rudolf, B., T. Fuchs, U. Schneider, and A. Meyer-Christoffer, 2003: Introduction of the Global Precipitation Climatology Centre (GPCC), Deutscher Wetterdienst, Offenbach a.M.; pp 16.
- Ryan, B., J. Katzfey, D.J. Abbs, C. Jakob, U. Lohmann, B. Rockel, L.D. Rotstayn, R.E. Stewart, K.K. Szeto, G. Tselioudis, and M.K. Yau, 2000: Simulations of a cold front by cloud-resolving, limited area and large-scale models, and a model evaluation using in-situ and satellite observations. *Mon. Wea. Rev.*, **128**, 3218–3235.
- Schneider, U. and Rudolf, B., 2003: Global Precipitation Climatology Centre. Report on the GEWEX-Meeting on “Objective Analyses of Precipitation” Reading/UK.
- Skelly, W.C. and A. Henderson-Sellers, 1996: Grid-box or grid-point: what type of precipitation data do GCMs deliver? *Int. J. Climatol.*, **16**, 1079–1086.
- Takle, E.S., J. Roads, B. Rockel, W.J. Gutowski, R.W. Arritt, I. Meinke, C.G. Jones, and A. Zadra, 2006: Transferability intercomparison: An opportunity for new insight on the global water cycle energy budget. *Bull. Amer. Meteor. Soc.* (accepted June 2006).
- Takle, E.S., W.J. Gutowski, R.W. Arritt, Z.T. Pan, C.J. Anderson, R.R. da Silva, D. Caya, S.-C. Chen, F. Giorgi, J.H. Christensen, S.Y. Hong, H.-M.H. Juang, J. Katzfey, W.M. Lapenta, R. Laprise, G.E. Liston, P. Lopez, J. McGregor, R.A. Pielke, and J.O. Roads, 1999: Project to Intercompare Regional Climate Simulations (PIRCS): Description and initial results. *JGR-Atmospheres* **104** (D 16), 19443–19461.
- Vidale, P.L., D. Lüthi, C. Frei, S.I. Seneviratne, and C. Schär, 2003: Predictability and uncertainty in a regional climate model. *JGR*, **2003**, 108, (D18), 4586, doi:10.1029/2002JD002810.
- von Storch, H. and F. Zwiers, 1999: *Statistical analysis in climate research*. Cambridge University Press, 484 pp.
- Wang, W. and N.L. Seaman, 1997: A comparison study of convective parameterization schemes in a mesoscale model. *Mon. Wea. Rev.*, **125**, 252–278.
- Zhang, G.J. and N.A. McFarlane, 1995: Sensitivity of climate simulations to the parameterization of cumulus convection in the Canadian Climate Centre general circulation model. *Atmos.–Ocean*, **33**, 407–446.